One-dimensional finite element formulation with node-dependent kinematics

E. Carrera[a,1], E. Zappino[a,2,*]

[a] *Politecnico di Torino, Mechanical and Aerospace Engineering Department, Corso Duca degli Abruzzi 24, 10129 Turin, Italy.*

Abstract

The present paper presents a refined one-dimensional finite element model with node-dependent kinematics. When this model is adopted, the beam theory can be different at each node of the same element. For instance, in the case of a 2-node beam element the Euler-Bernoulli theory could be used for node 1 and the Timoshenko beam theory could be used for node 2. Classical and higher-order refined models have been established with the Carrera Unified Formulation. Such a capability would allow the kinematic assumptions to be continuously varied along the beam axis, that is, no *ad hoc* mixing techniques such as the Arlequin method would be required. Different combinations of structural models have been proposed to account for different kinematic approximations of beams, and, beam models based on the Taylor and the Lagrange expansions have in particular been used. The numerical model has been assessed, and a number of applications to thin-walled

*Corresponding author

Email addresses: erasmo.carrera@polito.it (E. Carrera), enrico.zappino@polito.it (E. Zappino)

[1] Full Professor.

[2] Assistant Professor.

structures have been proposed. The results have been compared with those obtained from uniform kinematic models and convergence analyses have been performed. The results show the efficiency of the proposed model. The high accuracy of refined one-dimensional models has been preserved while the computational costs have been reduced by using refined models only in those zones of the beam that require them.
Keywords: CUF, node-dependent kinematic, FEM, one-dimensional mdoels

1. Introduction

Improvements in the performances of next-generation structures will require the use of new computational tools that are able to deal with multi-field problems and to provide increasingly accurate results. Classical one-dimensional structural models are used widely in the design of complex structures but they are limited by their fundamental assumptions. When the Euler-Bernoulli (Euler, 1744) beam model is used, it is accepted that the solution can only be considered accurate for slender bodies and isotropic materials. If moderately stubby structures are considered the model proposed by Timoshenko (1921) has to be used to include shear effects, and in this case, the use of a shear correction factor, see Timoshenko (1921); Cowper (1966); Dong et al. (2010), is required to overcome the approximation of a constant shear distribution over the cross-section. The de Saint-Venant principle (de Saint-Venant, 1856) states that two statically equivalent loads produce equivalent stress and strain fields if they are evaluated at a sufficiently large distance from the loads. In other words, even though the fundamental

assumption of classical models are satisfied, the loads and boundary condition may afflict the solution at a local level. Some examples can be seen in the works by Horgan and Simmonds (1994), Tullini (1997) and Lin et al. (2001) regarding end-effects or by Bar-Yoseph and Avrashi (1988) and by Bar-Yoseph and Ben-David (1995) concerning the free edge singularity. Advanced models are therefore required to obtain reliable results in that portion of the structure.

The introduction of refined structural models allows the limitations introduced by the fundamental assumptions of the classical models to be overcome and the stress singularities due to local effects to be dealt with. Many refined one-dimensional models have been proposed over the last few decades, e.g. the use of warping functions, as proposed by Vlasov (1961), allows the cross-section deformation to be included in the beam models. Cross-sectional warping plays an essential role in thin-walled structures as shown in the work by Friberg (1985) and Ambrosini (2000), where the warping function approach was used. Schardt (1966) proposed a one-dimensional model for the thin-walled structures analysis where the displacement field was considered as an expansion around the mid-plane of the thin-walled cross-section. This approach, which is called the generalized beam theory (GBT), was used by Davies and Leach (1994) and Davies et al. (1994), and an extension to the analysis of composite material was proposed by Silvestre and Camotim (2002). The Variation Asymptotic Method, VAM, proposed by Berdichevsky (1976), uses a characteristic cross-section parameter to build an asymptotic expansion of the solution. The application of this approach to one-dimensional structures can be seen in the work by Giavotto et al. (1983).

Volovoi (1999), Yu et al. (2002) and Yu and Hodges (2004) have extended this method to composite materials and beams with arbitrary cross-sections. Živković et al. (2001) proposed a general beam formulation including the cross-sectional deformation. A similar approach has been used by Yoon et al. (2012) and Yoon and Lee (2014) that proposed the introduction of a cross-sectional refined kinematic able to deal with in- and out-of-plane warping.

Different computational models have been developed on the basis of the above mentioned structural theories. A numerical tool that is frequently used in structural analysis is the Finite Element Model, FEM, which allows the structural theory to be easily included in the computational code. FEM models usually include classical structural theory, Timoshenko in the beam case, but also try to include refined approaches. This is the case of the so called elements BEAM188 and BEAM189 that exploit a cross-sectional model to define *ad-hoc* warping functions for each geometry, has proposed by Schulz and Filippou (1998). A unified formulation that is able to provide any order structural model has been proposed by Carrera (1995). This approach, called the Carrera Unified Formulation, CUF, has been used to derive both 1D (Carrera et al., 2010) and 2D (Carrera, 2002) theories. When one-dimensional models are considered, the CUF allows the cross-sectional displacement field to be described using a function expansion, and the accuracy of the results can be increased by just increasing the expansion order (Carrera et al., 2012b). In most cases, refined models are required to describe local effects when high stress gradients are present. In other cases, the classical model assumptions are not satisfied in some regions of the structure. The use of a refined beam model over the whole domain therefore requires

more computational costs than those necessary. The best solution would be to use refined models only in the region in which they are required and classical models elsewhere. The problem of *mixing* or *joining* different structural models is a well-known topic in literature. An exhaustive review of the state of the art can be found in the work by Wenzel (2014). When models with incompatible kinematics have to be joined, compatibility of the displacement should be imposed between the two domains. One of the possible approaches is to impose the compatibility condition at the boundary between the two models. Compatibility can be imposed using Lagrange multipliers, as shown in the work by Prager (1967); the same approach has been used in the frameworks of the CUF by Carrera et al. (2013). An extension of this approach was proposed by Ransom (2001) in which a spline was used to couple two incompatible meshes. This approach is called three-field. An alternative approach, which includes Lagrange multipliers in the principle of virtual work, was introduced by Blanco et al. (2008). A second approach that can be used to join incompatible structural models involves creating an overlapping zone of the two domains. In this case, there is a smooth transition between the two kinematics. An example of this approach is the Arlequin method, proposed by Ben Dhia and Rateau (2005); Ben Dhia (1998). In this case, compatibility in the shared area is imposed by using Lagrange multipliers. This approach has also been used in CUF frameworks, for example, in the work by Biscani et al. (2011). Finally, many approaches have been proposed that use a coarse mesh over the whole structure and only overlap a refined mesh in the area where complex phenomena are expected. Some examples are the s-FEM method proposed by Fish (1992) and the model proposed by Park

et al. (2003). The s-FEM method has been coupled with other refinement techniques, see Reddy and Robbins (1994), such as the p- and h- refinements, where the element order and the element size are refined locally. These refinement approaches were presented by Babuska and Chandra (1984), Szabo and Babuska (1991) and Rachowicz et al. (1989). Except for the cases mentioned above, the use of refined models based on the CUF has been limited to constant kinematic models, that is, the kinematic assumptions were considered uniform over the whole structural domain. The benefits, in terms of accuracy and computational cost, that came from the use of refined one-dimensional models, with respect to classical approaches, have been pointed out in many published works (Carrera and Petrolo, 2011; Carrera et al., 2012a) and will not be discussed here in detail. The present work has the aim to improve the efficiency of the well-know refined one-dimensional models introducing a node-dependent kinematic formulation able to adopt advanced kinematics only where required. This approach, in contrast with classical FE models, allows the accuracy to be improved using a refinement in the kinematic assumptions without any mesh refinement of the FEM model. This approach, in fact, allows different kinematics to be assumed at each node of a one-dimensional beam element. This permits: the accuracy of the model to be increased only in the part of the structure where this is required, a transition element to be created that is able to connect elements with different kinematics, classical beam models to be connected with shell and solid elements without any displacement discontinuities, as shown by Carrera and Zappino (2016) that connect refined one-, two- and three-dimensional models, and global-to-local analysis to be performed with only one model. No *ad hoc*

formulations have been introduced to achieve these results, the transition between different kinematics is in fact guaranteed by the shape functions used in the FE model. The use of the Carrera Unified Formulation, presented in (Carrera et al., 2014a), and the properties of the FEM allow the model to be derived in a compact form, which is called *fundamental nucleus*. This approach was presented in part by Carrera and Zappino (2014), some preliminary results were shown in that work. The present paper extends the approach to different beam models, and provides an exhaustive and general theoretical formulation. Classical models and equivalent single layer models, see (Carrera et al., 2010), based on a Taylor expansion, have been used where a low accuracy was required. Layer-wise models, see (Carrera E. and Petrolo, 2012), have instead been used where a refined result was required. The theoretical model is presented in the first part of the paper. Several results have been proposed to assess the model. Finally an application to the thin-walled structures has been introduced. The results show the advantages introduced by the present model, in terms of computational cost and accuracy.

2. Node-dependent kinematic beam elements

The one-dimensional finite element introduced in the following sections allows different kinematics to be used at each beam node. If a 2-node element is considered, see Figure 1, the kinematic assumptions used at node 1 can be different from those used at node 2. The capabilities of this element allow refined beam models to be used only at the beam nodes that require refined kinematics. Such features make the present element suitable for many applications: global to local analysis, transition elements, connection between

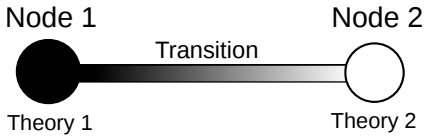

Figure 1: A two-nodes beam element with a node-dependent kinematic.

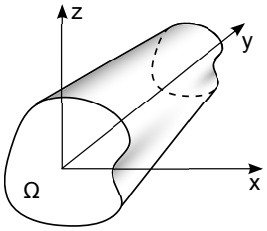

Figure 2: Reference system of the beam model.

different FEM models (1D to 2D or 2D to 3D). The use of a finite element formulation makes it possible to have a continuous transition of the kinematic assumption within the element without the need of any *ad hoc* formulation. The reference system shown in Fig. 2 is considered. The coordinate y stays on the axis of the beam while x and z lay on the cross-section Ω. The displacement vector can be written as:

$$\mathbf{u}^T = (u_x,\, u_y,\, u_z) \tag{1}$$

Where u_x, u_y and u_z are the displacement components in the three directions. The strains and stresses vectors are defined as:

$$\boldsymbol{\varepsilon}^T = (\varepsilon_{xx}, \varepsilon_{yy}, \varepsilon_{zz}, \varepsilon_{xy}, \varepsilon_{xz}, \varepsilon_{yz}), \tag{2}$$

$$\boldsymbol{\sigma}^T = (\sigma_{xx}, \sigma_{yy}, \sigma_{zz}, \sigma_{xy}, \sigma_{xz}, \sigma_{yz}). \tag{3}$$

The relation between strains and displacements can be written using the geometrical equation:

$$\boldsymbol{\varepsilon} = \boldsymbol{D}\boldsymbol{u}, \tag{4}$$

where $\boldsymbol{D}$ is a differential operator, the explicit form of $\boldsymbol{D}$ can be found in (Carrera et al., 2014a). The Hooke's law permits to derive the relation between stresses and strains:

$$\boldsymbol{\sigma} = \boldsymbol{C}\boldsymbol{\varepsilon}, \tag{5}$$

where $\boldsymbol{C}$ is the stiffness coefficients matrix of the material.

2.1. Review of one-dimensional model kinematic assumptions

The kinematic assumptions of some classical and refined beam models are briefly introduced in the following sections.

2.1.1. Classical beam models

Classical beam models are subject to a number of fundamental assumptions that limit the use of these models to a small number of applications.

The Euler-Bernoulli beam theory, EBBT, does not consider shear effects and the warping of the cross-section, which is considered rigid in- and out-of-plane. The displacement field of the cross-section can be written as:

$$\begin{aligned} u_x &= u_{x_1} \\ u_y &= u_{y_1} + x\,\frac{\partial u_{z_1}}{\partial y} + z\,\frac{\partial u_{x_1}}{\partial y} \\ u_z &= u_{z_1} \end{aligned} \tag{6}$$

This model has only three degrees of freedom, DOF, over the cross-section

because the rotation of the cross-section is considered as the derivatives of the rigid translation.

The Timoshenko beam theory, TBT, includes the effects of the shear but it is considered constant over the cross-section. In this case, the displacement field of the cross-section can be written as:

$$\begin{aligned} u_x &= u_{x_1} \\ u_y &= u_{y_1} + x\, u_{y_2} + z\, u_{y_3} \\ u_z &= u_{z_1} \end{aligned} \tag{7}$$

The TBT has five DOFs, because the cross-sectional rotation is a free parameter. The use of these models is limited to slender (EBBT) and moderately slender (TBT) bodies, because the fundamental assumptions are only verified for these geometries. In the present form these models can be used to describe the bending of prismatic beam. The torsional effects can be included considering the contributions introduced by de Saint-Venant (1856) or, in the case of thin-walled structures, by Vlasov (1961).

The use of refined one-dimensional models allows the range of applicability of these models to be extended to a large number of applications. In this work the refined one-dimensional models derived from using the CUF are used to build node-dependent kinematic one-dimensional models. A brief review of these models is presented in the following section.

2.1.2. Refined one-dimensional models

The one-dimensional approximation requires a known displacement field to be assumed over the cross-section. A function expansion can be used

to describe properly the behavior of the beam cross-section. This approach, suggest by Washizu (1968), leads to write the three-dimensional displacement field as:

$$\mathbf{u} = \mathbf{u}_\tau(y) F_\tau(x, z), \qquad \tau = 1 \dots M. \tag{8}$$

where $F_\tau(x, z)$ is the function expansion over the cross-section, $\mathbf{u}_\tau(y)$ is the unknown vector along the beam axis, and M is the number of terms in the functions expansion $F_\tau(x, z)$. The choice of the functions expansion allows the kinematic of the model to be modified. A number of possible choices were presented by Carrera et al. (2014b). In the present work Taylor and Lagrange expansions are considered, more details are reported in the next sections.

The displacements approximation introduced in Eq.8 leads to a one-dimensional problem. The solution of this problem can be obtained using the Finite Element Method, FEM, which allows the system of partial derivative functions to be reduced to an algebraic system. FEM approximates the axial unknowns $\mathbf{u}_\tau(y)$ using the one-dimensional shape functions N_i, that is, the displacement field assumes the formulation:

$$\mathbf{u} = \mathbf{u}_{i\tau} N_i(y) F_\tau(x, z), \qquad \tau = 1 \dots M; \qquad i = 1 \dots N_n. \tag{9}$$

where N_i are the shape functions introduced by the FE model, N_n is the number of nodes of the element and $\mathbf{u}_{i\tau}$ are the nodal unknowns. The virtual variation of the displacement can be written as:

$$\delta\mathbf{u} = \delta\mathbf{u}_{js} N_j(y) F_s(x, z), \qquad s = 1 \dots M; \qquad j = 1 \dots N_n. \tag{10}$$

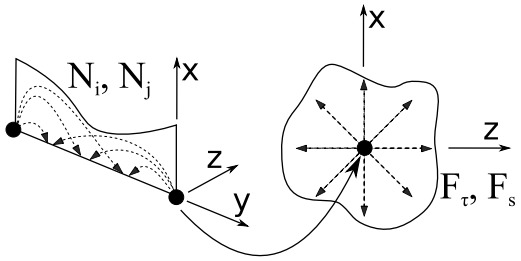

Figure 3: A two-nodes beam based on the Taylor expansion.

2.1.3. Taylor expansion models (TE)

The one-dimensional TE model consists of an expansion that uses 2D polynomials $x^m\ z^n$, as F_τ, where m and n are positive integers. For instance, the second-order displacement field is:

$$\begin{aligned} u_x = &\ u_{x_1} + x\,u_{x_2} + z\,u_{x_3} + x^2\,u_{x_4} + xz\,u_{x_5} + z^2\,u_{x_6} \\ u_y = &\ u_{y_1} + x\,u_{y_2} + z\,u_{y_3} + x^2\,u_{y_4} + xz\,u_{y_5} + z^2\,u_{y_6} \\ u_z = &\ u_{z_1} + x\,u_{z_2} + z\,u_{z_3} + x^2\,u_{z_4} + xz\,u_{z_5} + z^2\,u_{z_6} \end{aligned} \tag{11}$$

Figure 3 shows a representation of a two nodes element based on the TE expansion. In this case, the F_τ and F_s functions are used to expand the solution from the beam node to the cross-section.

2.1.4. Lagrange expansion models (LE)

In the case of LE models, Lagrange polynomials are used to build refined one-dimensional models. The iso-parametric formulation is exploited to deal with arbitrary cross-section shaped geometries. For instance, the linear in-

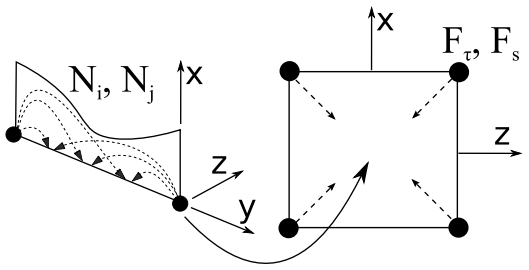

Figure 4: A two-nodes beam based on the Lagrange expansion.

terpolation functions are:

$$F_1 = \tfrac{1}{4}(1-\xi)(1-\eta); \quad F_2 = \tfrac{1}{4}(1+\xi)(1-\eta);$$
$$F_3 = \tfrac{1}{4}(1+\xi)(1+\eta); \quad F_4 = \tfrac{1}{4}(1-\xi)(1+\eta) \tag{12}$$

where ξ and η are the coordinates in the natural reference system. Equation 12 coincides with the linear Lagrange polynomial in two dimensions. In this paper a quadratic element with nine nodes, LE9, is used. When LE is used the unknowns are only the displacements of the cross-sectional nodes.

Figure 4 shows a representation of a two nodes element based on the LE. In this case the F_τ and F_s functions are used to expand the solution from the cross-sectional nodes to the cross-section area.

3. Formulation of a one-dimensional Finite Element with node-dependent kinematics

When the geometry or boundary conditions of a structure are outside the range of applicability of classical beam models, higher-order models can

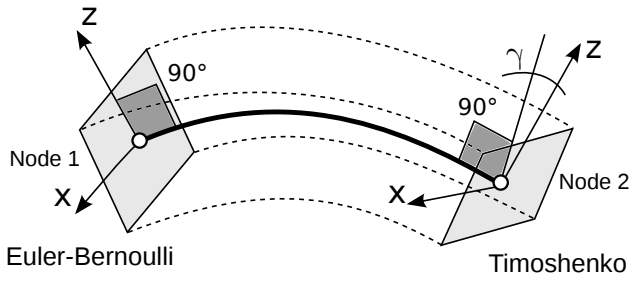

Figure 5: Two node beam element with the Euler-Bernoully kinematic assumptions at node 1 and Thimoshenko kinematic assumptions at node 2.

be used to improve the solution and overcome their limitations. The use of refined kinematic models increases the accuracy of the models in each part of the considered domain. Therefore, a higher computational cost is required.

In most cases, a refined kinematics is required only in some parts of the domain, where local effects appear, while classical models could be used elsewhere. Figure 5 shows the simple case of a 2-node element. An Euler-Bernoulli kinematic is used at node 1 while a Timoshenko beam model is used at node 2 because some shear effects can be present.

A more generic configuration is shown in Figure 6. Some sections undergo bending phenomena, and a classical model can therefore be used. Other sections are slightly deformed, and a low-order refined beam model can be used in these sections. Finally, some sections could show large in- and out-of-plane warping, and as a result, a higher-order model is required in these part of the structure.

A new class of node-dependent kinematic elements is introduced in this work to refine the kinematics only in the part where it is required.

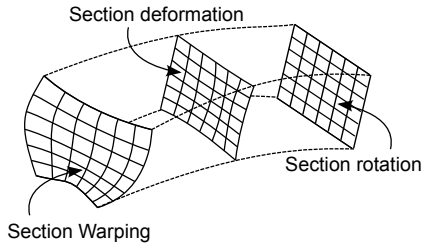

Figure 6: beam under a general deformation configuration.

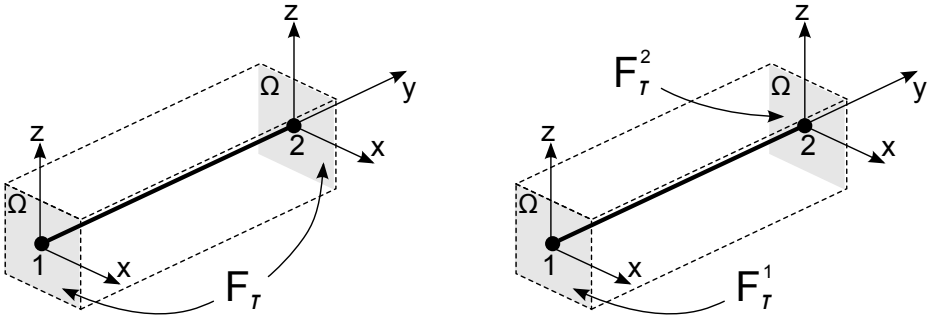

(a) Refined Beam Model

(b) Variable Kinematic Refined Beam Model

Figure 7: Cross-sectional approximation of different refined beam models.

3.1. A two-node element with node-dependent kinematics

A two-node one-dimensional element is considered in this section. Refined beam models with constant kinematic assume the same cross-sectional expansion in both nodes, as shown in Figure 7a. If the problem suggests that a more complex solution should be investigated in one of the nodes, a more refined kinematics can be introduced only in that node, that is, two different expansion should be used, see Figure 7b. The use of the FE method and the introduction of the shape functions allows a different displacement field to be considered at each node. The displacement field at the first node can be written as:

$$\mathbf{u}^1 = \mathbf{u}_{1\tau} F_\tau^1, \qquad \tau = 1 \dots M^1 \tag{13}$$

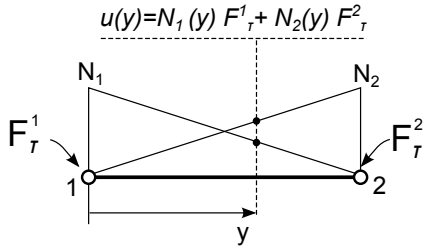

Figure 8: Displacement field of a node-dependent kinematic beam element.

while, the displacement field at the second node is:

$$\mathbf{u}^2 = \mathbf{u}_{2\tau} F_\tau^2, \qquad \tau = 1 \dots M^2 \tag{14}$$

The three-dimensional displacement field of the whole element, as shown in Figure 8, becomes:

$$\mathbf{u} = \mathbf{u}_{1\tau} N_1 F_\tau^1 + \mathbf{u}_{2\tau} N_2 F_\tau^2, \qquad \tau = 1 \dots M^i \tag{15}$$

If a first order Taylor expansion is used at the first node, and a second order Taylor expansion is used at the second node, the displacement field becomes:

$$\mathbf{u} = N_1 \underbrace{\left[\mathbf{u}_1^1 + \mathbf{u}_2^1 x + \mathbf{u}_3^1 z\right]}_{1^{st} node} + N_2 \underbrace{\left[\mathbf{u}_1^2 + \mathbf{u}_2^2 x + \mathbf{u}_3^2 z + \mathbf{u}_4^2 x^2 + \mathbf{u}_5^2 xz + \mathbf{u}_6^2 z^2\right]}_{2^{nd} node} \tag{16}$$

The two different displacement fields are *smeared* by the shape functions that ensure a smooth transition between the displacement fields of the two nodes. Using this approach, the continuity of the displacement is ensured at each point. The same approach can be used using a Lagrange expansion at one of the two nodes. If a first-order Taylor expansion is considered at the first

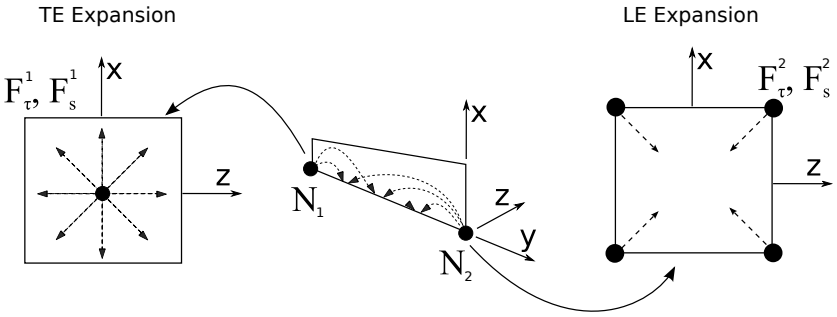

Figure 9: Two node element with a TE model on node 1 and a LE model on node 2.

node, and a 4-node Lagrange element is used at the second node, see Figure 9, the displacement field becomes:

$$\mathbf{u} = N_1 \underbrace{\left[\mathbf{u}_1^1 + \mathbf{u}_2^1 x + \mathbf{u}_3^1 z\right]}_{1^{st}node} + N_2 \underbrace{\left[\mathbf{u}_1^2 L_1 + \mathbf{u}_2^2 L_2 + \mathbf{u}_3^2 L_3 + \mathbf{u}_4^2 L_4\right]}_{2^{nd}node} \tag{17}$$

3.2. General formulation of a node-dependent kinematics element

The approach introduced in the previous section can be easily included in the CUF formulation and extended to any order beam model. The displacement field of the one-dimensional element with node-dependent kinematic can be written including two main novelties:

$$F_\tau(x,z) \longrightarrow F_\tau^i(x,z) \tag{18}$$

$$M \longrightarrow M^i \tag{19}$$

The first equation, Eq. 18, states that the function expansion is not a property of the element, but of the nodes, that is, the index i is included in the notation. Eq. 19 remarks that the number of terms in the expansion, M, can be different at each node, and the notation M^i is used to underline this

aspect. The generic displacement field can be written as:

$$\mathbf{u} = \mathbf{u}_{i\tau} N_i(y) F^i_\tau(x,z), \qquad \tau = 1 \dots M^i; \qquad i = 1 \dots N_n. \tag{20}$$

3.3. Governing Equations

The governing equations can be derived using the Principle of Virtual Displacements (PVD) which assumes the following form in the static case:

$$\delta L_{int} = \delta L_{ext} \tag{21}$$

where L_{int} stands for the strain energy, L_{ext} is the work of the external loadings and δ denotes the virtual variation. The internal work can be written as:

$$\delta L_{int} = \int_V \delta \boldsymbol{\epsilon}^T \boldsymbol{\sigma} dV \tag{22}$$

By introducing the constitutive equations and the geometrical relations given in Eq.4 and Eq.5 respectively, and introducing the displacement field given in Eq. 20, the variation in the internal work becomes:

$$\delta L_{int} = \delta \mathbf{q}^T_{sj} \int_V \left[N_j(y) F^j_s(x,z) \;\; \boldsymbol{D}^T \;\; \boldsymbol{C} \;\; \boldsymbol{D} \;\; F^i_\tau(x,z) N_i(y) \right] dV \mathbf{q}_{\tau i} \tag{23}$$

$$= \delta \mathbf{q}^T_{sj} \;\; \boldsymbol{K}^{ij\tau s} \;\; \mathbf{q}_{\tau i} \tag{24}$$

where $\boldsymbol{K}^{ij\tau s}$ is the stiffness matrix expressed in the form of a *fundamental nucleus* that is a 3×3 array, $\mathbf{q}_{\tau i}$ is the vector of the nodal unknown and $\delta \mathbf{q}_{sj}$ is its virtual variation. The fundamental nucleus, in the case of isotropic

material, can be written in the extended form as follows:

$$
\begin{aligned}
k_{xx}^{ij\tau s} = \; & C_{22}\int_{\Omega} F_{\tau,x}^{i}F_{s,x}^{j}d\Omega\int_{l} N_iN_jdy + C_{66}\int_{\Omega} F_{\tau,z}^{i}F_{s,z}^{j}d\Omega\int_{l} N_iN_jdy + \\
& C_{44}\int_{\Omega} F_{\tau}^{i}F_{s}^{j}d\Omega\int_{l} N_{i,y}N_{j,y}dy \\
k_{xy}^{ij\tau s} = \; & C_{23}\int_{\Omega} F_{\tau,x}^{i}F_{s}^{j}d\Omega\int_{l} N_iN_{j,y}dy + C_{44}\int_{\Omega} F_{\tau}^{i}F_{s,x}^{j}d\Omega\int_{l} N_{i,y}N_jdy \\
k_{xz}^{ij\tau s} = \; & C_{12}\int_{\Omega} F_{\tau,x}^{i}F_{s,z}^{j}d\Omega\int_{l} N_iN_jdy + C_{66}\int_{\Omega} F_{\tau,z}^{i}F_{s,x}^{j}d\Omega\int_{l} N_iN_jdy \\
k_{yx}^{ij\tau s} = \; & C_{44}\int_{\Omega} F_{\tau,x}^{i}F_{s}^{j}d\Omega\int_{l} N_iN_{j,y}dy + C_{23}\int_{\Omega} F_{\tau}^{i}F_{s,x}^{j}d\Omega\int_{l} N_{i,y}N_jdy \\
k_{yy}^{ij\tau s} = \; & C_{55}\int_{\Omega} F_{\tau,z}^{i}F_{s,z}^{j}d\Omega\int_{l} N_iN_jdy + C_{44}\int_{\Omega} F_{\tau,x}^{i}F_{s,x}^{j}d\Omega\int_{l} N_iN_jdy + \\
& C_{33}\int_{\Omega} F_{\tau}^{i}F_{s}^{j}d\Omega\int_{l} N_{i,y}N_{j,y}dy \\
k_{yz}^{ij\tau s} = \; & C_{55}\int_{\Omega} F_{\tau,z}^{i}F_{s}^{j}d\Omega\int_{l} N_iN_{j,y}dy + C_{13}\int_{\Omega} F_{\tau}^{i}F_{s,z}^{j}d\Omega\int_{l} N_{i,y}N_jdy \\
k_{zx}^{ij\tau s} = \; & C_{12}\int_{\Omega} F_{\tau,z}^{i}F_{s,x}^{j}d\Omega\int_{l} N_iN_jdy + C_{66}\int_{\Omega} F_{\tau,x}^{i}F_{s,z}^{j}d\Omega\int_{l} N_iN_jdy \\
k_{zy}^{ij\tau s} = \; & C_{13}\int_{\Omega} F_{\tau,z}^{i}F_{s}^{j}d\Omega\int_{l} N_iN_{j,y}dy + C_{55}\int_{\Omega} F_{\tau}^{i}F_{s,z}^{j}d\Omega\int_{l} N_{i,y}N_jdy \\
k_{zz}^{ij\tau s} = \; & C_{11}\int_{\Omega} F_{\tau,z}^{i}F_{s,z}^{j}d\Omega\int_{l} N_iN_jdy + C_{66}\int_{\Omega} F_{\tau,x}^{i}F_{s,x}^{j}d\Omega\int_{l} N_iN_jdy + \\
& C_{55}\int_{\Omega} F_{\tau}^{i}F_{s}^{j}d\Omega\int_{l} N_{i,y}N_{j,y}dy
\end{aligned}
\tag{25}
$$

The work done by the external loads can be written as:

$$
\delta L_{ext} = \int_{V} \delta \boldsymbol{u}^{T}\boldsymbol{P}dV \tag{26}
$$

where $\boldsymbol{u}$ is the displacement vector at one point and $\boldsymbol{P}$ is the load applied at that point. When a three-dimensional load is considered the external work can be written as:

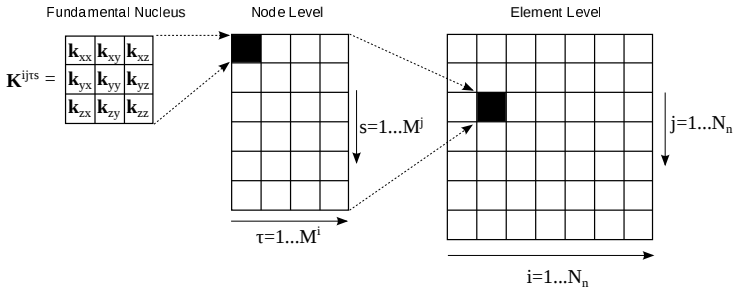

Figure 10: Stiffness matrix assembly.

$$\delta L_{ext} = \delta \mathbf{q}_{sj}^T \int_V \delta N_j(y) F_s^j(x,z) \boldsymbol{P} dV = \delta \mathbf{q}_{sj}^T \boldsymbol{P}^{js} \tag{27}$$

3.4. The matrix assembly

The fundamental nuclei introduced in the previous section, that are discussed extensively in (Carrera et al., 2014a), can be used as bricks to build the matrix of the complete structure. Figure 10 shows the procedure used to build the stiffness matrix, starting from the fundamental nucleus.

This approach has been introduced in many works by the authors (Carrera et al., 2014a) where the structural model has been considered constant at each beam element. In the present paper, the approximation used for each beam mode may be different. This aspect can be seen at the node level, that is, the loop on the τ and s indices can have a different number of terms and the matrix may therefore appear rectangular at this level. The dimensions of this block depend on the number of terms in the expansions in the i and j nodes. When $i = j$, the matrix at the node level is always square because $M^i = M^j$.

4. Numerical results

This section shows the results obtained using the node-dependent kinematic models presented in the previous sections. An assessment of the models is reported in the first part, and, these models are then used to investigate the response of a thin-walled structure.

4.1. Node-dependent kinematic model assessment

A simple supported compact beam has been considered to assess the structural model. First, a node-dependent kinematic TE model has been considered, and a variable order of expansion has therefore been considered for each node of the beam. A mixed TE/LE model has been considered as the second case. Let us consider the models reported in figure 11. It is a clamped-clamped beam with a rectangular compact cross-section, with height, h, of 0.1 m and width, b, of 0.2 m. The length of the beam is 1 m. An aluminium alloy is considered as the material, with a Young's modulus, E, of 71.7 GPa and a Poisson's ratio, ν, of 0.3.

The structure is loaded with force, P, with a magnitude of 100 N, at the mid-span of the beam. The results are reported in terms of displacements, a reference solution was obtained using a solid model (HEXA 8 elements), developed using the commercial FEM code MSC NASTRAN. Different solid models have been considered in order to see the effects of the three-dimensional mesh refinement. Table 1 shows the vertical displacement at the loading point and the number of degrees of freedom of the Solid models considered. The three-dimensional models are described using three numbers that describe the used mesh. As an example, model $3D^{2\times10\times1}$ was built us-

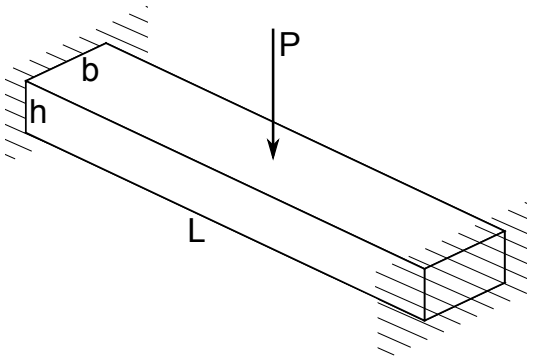

Figure 11: Geometry of the clamped-clamped beam.

Model	$u_z \times 10^{-7}$	$Err\%$	DOFs
$3D^{2\times10\times1}$	-4.610	-20.5	198
$3D^{4\times20\times2}$	-4.918	-15.2	945
$3D^{6\times30\times3}$	-5.240	-9.6	2604
$3D^{8\times40\times4}$	-5.526	-4.7	5535
$3D^{10\times50\times5}$	-5.798	0.0	10098

Table 1: Vertical displacement on the loading point evaluated using several three-dimensional models.

ing 2 elements along the dimension b, 10 elements over the beam length and 1 along the h dimension. The results obtained using the model $3D^{10\times50\times5}$ can be considered as the more accurate and therefore they will be used as reference values to assess the variable kinematic models.

Different models, based on the present one-dimensional formulation, are considered in the following section in order to investigate the performance of the variable kinematic element introduced in this work. First, a classical formulation, Euler-Bernoulli, and various refined TE models (from TE-2 to TE-19) are used to study the convergence of the results. Then the node-dependent kinematic models, first TE/TE and then TE/LE are then introduced to evaluate the performances of these approaches.

4.1.1. Node-dependent kinematic TE/TE models

A convergence analysis has been performed in order to evaluate the effect of the expansion order on the accuracy of the results. Different TE models were considered, from TE-2 to TE-19, including the Euler model (EULE). Six cubical beam elements (B4) have been considered in this case. The results, in terms of displacement at the loading point, are reported in tab. 2. The results show as the order of the model is increased, the solution converges to the reference solution, and the error is only the 8.2% for a TE-19 model. The classical model, EBBT, gives a larger error than 20%, because it is not able to predict the local effects that appear where the load is applied. The use of refined models increases the accuracy but, at the same time, increases the number of degrees of freedom required for the analysis.

The central part of the beam undergoes a remarkable cross-section deformation, and for this reason a higher-order model is required to properly

Model	$u_z \times 10^{-7}$	$Err\%$	DOFs
EBBM (Analytical)	-4.358	-24.8	-
EULE	-4.359	-24.8	171
TE-2	-4.618	-20.3	342
TE-3	-4.743	-18.2	570
TE-4	-4.815	-16.9	855
TE-5	-4.864	-16.1	1179
TE-6	-4.912	-15.3	1596
TE-7	-4.954	-14.5	2052
TE-8	-4.995	-13.8	2565
TE-11	-5.105	-11.9	4446
TE-16	-5.243	-9.6	9639
TE-19	-5.321	-8.2	13230
$3D^{10\times50\times5}$	-5.798	-	10098

Table 2: Vertical displacement at the loading point for different TE structural models.

evaluate the displacements of this portion of the structure. However, the part of the beam close to the constraints can be analyzed with a lower-order model, because the cross-section deformation is limited.

In order to reduce the computational cost, and increase the accuracy of the results, a node-dependent kinematic model could be introduced, as this would lead to accurate results if the refined model were just used where needed.

Figure 12 shows the node-dependent kinematic model used in the analysis. The two parts close to the boundary condition only require a TE-2 model, while the central part has been analyzed using a refined model. A linear beam element (B2), with node-dependent kinematics was used to join the different parts of the model.

Different refined models have been considered in the central part of the

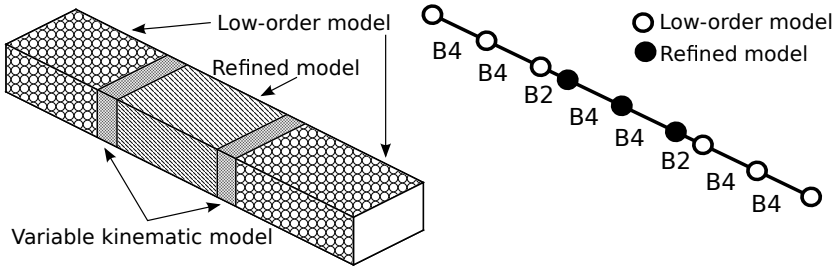

Figure 12: Description of the node-dependent kinematic model.

Model	$u_z \times 10^{-7}$	$Err\%$	DOFs
EBBM (Analytical)	-4.358	-24.8	-
EULE	-4.359	-24.8	171
TE-2/TE-4	-4.767	-17.8	567
TE-2/TE-6	-4.862	-16.1	840
TE-2/TE-9	-4.988	-14.0	1402
TE-2/TE-19	-5.256	-9.3	4662
$3D^{10\times50\times5}$	-5.798	-	10098

Table 3: Vertical displacement on the loading point evaluated using the node-dependent kinematics models.

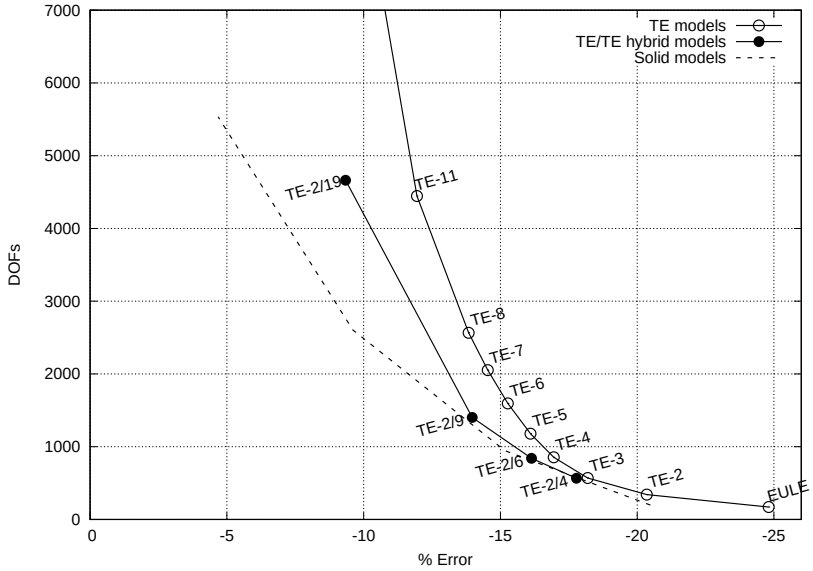

Figure 13: Error vs DOFs for node-dependent kinematics TE/TE models.

structure. The results for the TE-2/TE-4, TE-2/TE-6, TE-2/TE-9 and TE-2/TE-19 models are reported in Table 3. The results show how the node-dependent kinematic models are able to provide accurate results with a low number of degrees of freedom. The TE-2/TE-19 model provides almost the same accuracy as the TE-19 model, but it only uses 4662 DOFs instead of 13230. The same results are reported in Figure 13. Constant kinematic models show convergence but, the computational cost increases dramatically when the error becomes smaller. The use of node-dependent kinematic models allows the same accuracy to be reached with a lower number of degrees of freedom. It should be noted that the present approach does not require any *ad hoc* tool to couple the different kinematic models and it only use the features of the finite element model. The results obtained using the solid models are still more accurate because of their capabilities to describe the

local effects. The introduction of a LE model could increase the accuracy of the present one-dimensional model.

4.1.2. Node-dependent kinematic TE-LE models

The use of LE models allows local effect to be investigated efficiently. The capabilities of these LE models have been shown in many works, see (Carrera E. and Petrolo, 2012). The use of TE models coupled with LE models, seems to be very promising when local effects have to be investigated. In the present section, the variable TE/LE model is used to analyze the same structure that was analyzed before.

The model shown in Figure 12 is used once again, but, in this case the central part is solved using a refined model based on LE expansion. Different cross-sectional discretization have been considered. Model $LE-2Q9$ only uses 2 $Q9$ elements over the cross-section, while $LE-16Q9$ uses 16 $Q9$ elements. Models $LE-4Q9$ and $LE-8Q9$ use 4 and 8 $Q9$ elements respectively. The constant kinematic models based only on LE expansion have also been included in the analysis for comparison purposes.

The results are reported in Table 4. The use of an LE model provide very accurate results; the $LE-8Q9$ model has almost the same accuracy as the $TE-19$ model, but has a lower number of DOFs.

The introduction of a node-dependent kinematic model, TE-2/LE-2Q9 to TE-2/LE-16Q9, leads to very accurate results, but with a strong reduction in the computational cost. The $TE-2/LE-16Q9$, in fact, provides accurate results using only 2037 DOFs while the constant kinematic $LE-16Q9$ has 5355 DOFs and the the reference model $3D^{10\times50\times5}$ has 10098 DOFs.

The results are reported in Figure 14, where the errors and number of

Model	$u_z \times 10^{-7}$	$Err\%$	DOFs
LE-2Q9	-5.097	-12.1	855
LE-4Q9	-5.253	-9.4	1701
LE-8Q9	-5.355	-7.6	3213
LE-16Q9	-5.663	-2.3	5355
TE-2/LE-2Q9	-5.037	-13.1	567
TE-2/LE-4Q9	-5.241	-9.6	819
TE-2/LE-8Q9	-5.343	-7.8	1323
TE-2/LE-16Q9	-5.612	-3.2	2037
$3D^{10\times50\times5}$	-5.798	-	10098

Table 4: Vertical displacement on the loading point for node-dependent kinematics TE/LE models.

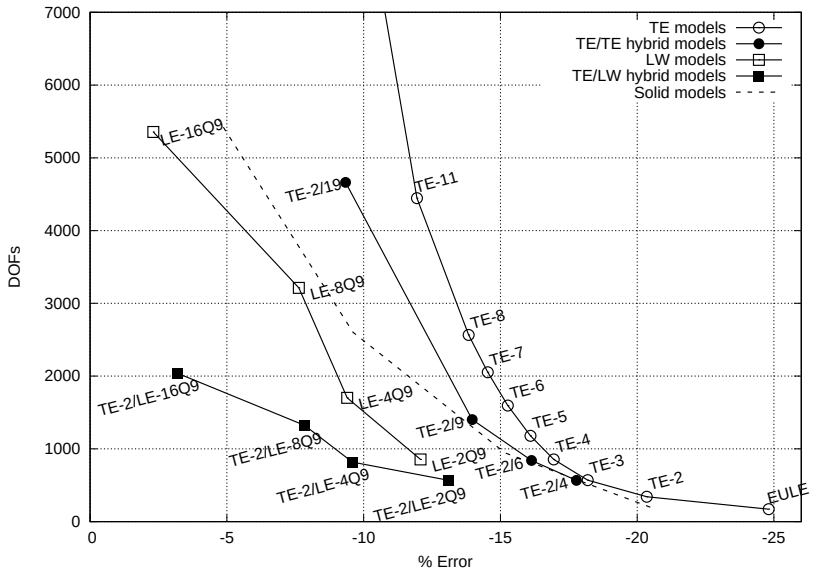

Figure 14: Error vs DOFs for node-dependent kinematics TE/LE models.

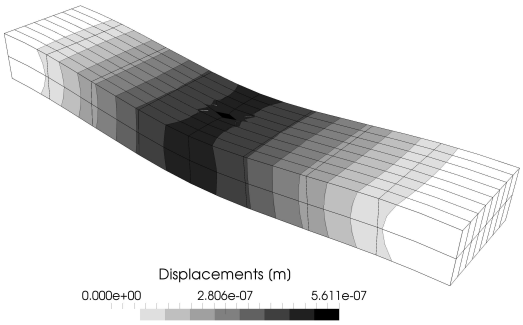

Figure 15: Displacements field obtained using the $TE-2/LE-16Q9$ model.

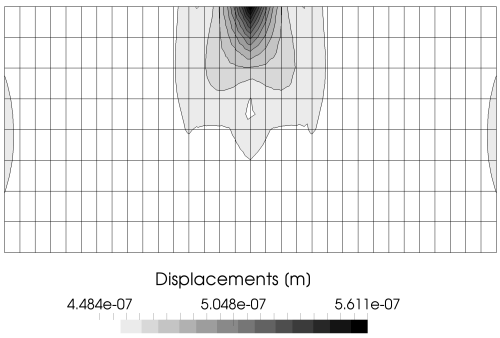

Figure 16: Displacement field of the loaded cross-section evaluated using the $TE-2/LE-16Q9$ model.

DOFs are compared. The node-dependent kinematic models appear to be much more efficient than the constant kinematic one. The coupling between the high accuracy of the LE models and the low computational cost of the TE model provides the best solution.

Figure 15 shows the deformation of the beam using $LE-16Q9$ model. The solution shows how, even when this simple structural configuration is considered, the displacement field evaluated using a classical model is not accurate, because of the local effects due to the load application. Figure 16 shows the displacement field over the cross-section where the load is applied.

This result shows how the load produces a local deformation that can not be detected with classical models that consider a rigid cross-section.

4.2. Thin walled structure analysis

A thin-walled structure has been considered in this section to evaluate the performances of a node-dependent kinematic model when complex structures are considered.

A cantilevered beam with a C-shaped cross-section has been considered. The geometry is reported in Figures 17 and 18. The beam has a length, l, of 1 m, a height, h, of 0.1 m and the wall of the section has a thickness, t, of 0.005 m. The considered material is aluminium alloy, as in the previous case. Eight B4 elements are used in the FE model, as shown in Figure 17. When an LE model is considered, nine-node elements have been used over the cross-section. Three meshes have been considered, the first uses five Q9 elements, LE-5Q9, the second uses eight Q9 elements, LE-8Q9, and finally a mesh with ten Q9 elements, LE-10Q9, has been considered. The cross-sectional meshes can be seen in Figure 19.

The structure has been loaded at its tip with two different load configurations. Load case 1 , shown in figure 18, has two loads at points A and B with the same magnitude, 1000 N, but in the opposite direction. The second has only a vertical load of 1000N at point B, as shown in Figure 18.

A convergence analysis has been performed to identify which refined one-dimensional model is able to predict correctly the solution.

Table 5 shows the results obtained using different refined one-dimensional models with a uniform kinematic. A reference solution has been obtained using a shell model solved using the commercial code Nastran. The results

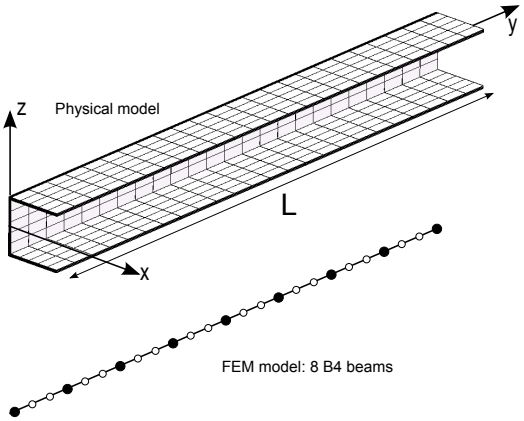

Figure 17: Thin-walled beam geometry and FEM model.

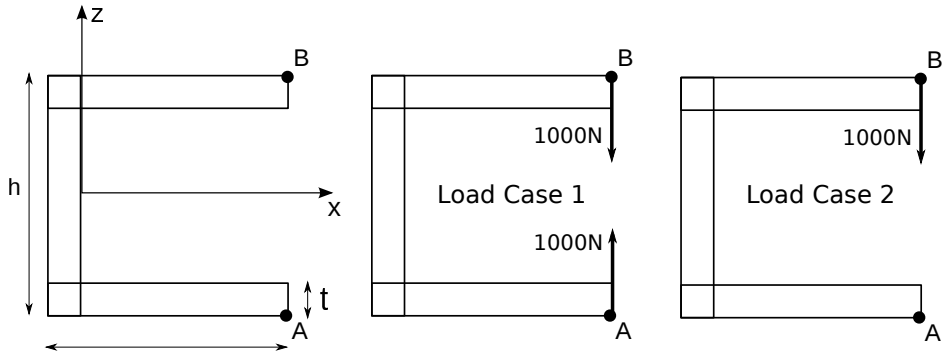

Figure 18: Cross-sectional geometry and load cases.

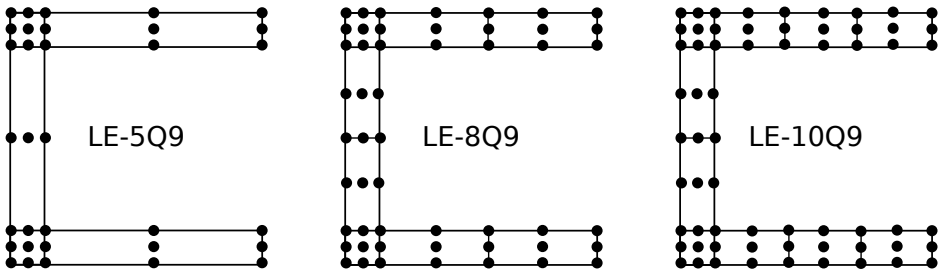

Figure 19: LE models cross-sectional discretization.

	Load Case 1	Load Case 2		
Model	$u_z^B \times 10^{-3}$[m]	$u_z^B \times 10^{-2}$[m]	$u_z^A \times 10^{-2}$[m]	NDOF
LE-5Q9	-7.382	-2.663	-1.925	2475
LE-8Q9	-7.814	-2.712	-1.931	3825
LE-10Q9	-7.906	-2.721	-1.930	4725
TE-1	-0.002	-0.141	-0.141	225
TE-2	-0.011	-0.187	-0.186	450
TE-3	-0.048	-0.205	-0.200	750
TE-4	-0.454	-0.555	-0.510	1125
TE-5	-0.916	-0.662	-0.570	1575
TE-6	-4.089	-0.662	-0.570	2100
TE-7	-5.031	-1.826	-1.323	2700
TE-8	-5.693	-2.180	-1.611	3375
TE-10	-6.666	-2.376	-1.709	4950
TE-14	-7.412	-2.627	-1.885	9000
Reference	-8.080	-2.782	-1.974	7500

Table 5: Vertical displacement evaluated using different uniform kinematic refined models.

show that, when load case 1 is considered and even if a high-order TE model is used, the results are still far from the reference solution. The use of a LE model is mandatory to capture the local effects. $LE-10Q9$ model is able to predict the vertical displacement with an error lower than 2.2%.

When load case 2 is considered the results show that the TE models can provide accurate results only with very high-order models, see TE-14, but using a large number of degrees of freedom. Once again, the use of LE models could lead to accurate results with a lower computational cost, in this case the model LE-8Q9 is able to provide results with an error lower than 2.5%.

Model $LE-10Q9$ and $LE-8Q9$ will be used as a reference for the load case 1 and the load case 2 respectively.

The use of a node-dependent kinematic may lead to a reduction in the computational costs. For the load case 1, models based on $LE-10Q9$ and $TE-2$ kinematic assumptions have been considered while, for load case 2, $LE-8Q9$ and $TE-4$ kinematic models have been taken into account.

The full LE model, which provides the most accurate results but also the highest computational cost, has been used as a reference. The TE model has the been introduced, starting from the root of the beam. The number of TE elements has been increased until the model has become a full TE model.

Figure 20 shows the displacement fields for case loads 1 and 2. When load case 1 is considered, the deformation is local, and only involves the cross-section, 20a. Load case 2, shown in 20b, produces torsion of the beam, and the deformation is more global.

Table 6 shows the results for the load case 1. The first 8 columns show the structural model used for each element of the beam. The model in the

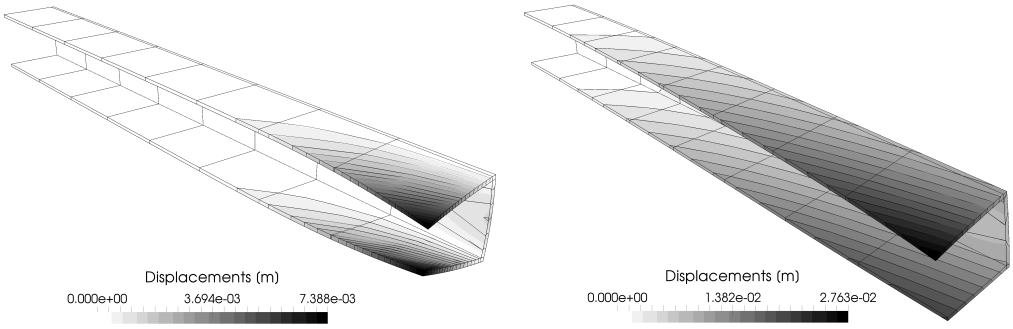

(a) Displacement field under load case 1 (b) Displacement field under load case 2

Figure 20: Displacement field evaluated using a full LE model.

first line, where only stars are reported, is a full LE model. A full TE-2 model is considered in the last line, where only triangles appear. Lines 2 to 7 report the node-dependent kinematic models in which a mixed TE-2/LE-10Q9 model is used. The last two columns report the displacement value at point A (which, for symmetry reasons, is equal to the displacement at point B) and the number of DOFs used in the model.

The results show that the use of a node-dependent kinematic model allows the computational cost to be reduced. Since the local effects due to the load case 1 only appear at the tip of the structure, a refined LE model is only required for the last three elements. The use of an LE model over the entire beam is a waste of DOFs, while, the use of a full TE-3 model does not allow accurate results to be reached.

Table 7 reports the same results for load case 2. The table reports the displacement at both points A and B. In this case the use of a higher order model is required over the whole beam. Since TE-4 model is not accurate enough to describe such deformation, it could be used only in the first element. In all the other cases, the use of a TE-4 model is not sufficient to

Structural model for each element									
El.1	El.2	El.3	El.4	El.5	El.6	El.7	El.8	$u_A \times 10^{-3}$[m]	DOFs
★	★	★	★	★	★	★	★	-7.906	4725
△	★	★	★	★	★	★	★	-7.906	4212
△	△	★	★	★	★	★	★	-7.906	3699
△	△	△	★	★	★	★	★	-7.906	3186
△	△	△	△	★	★	★	★	-7.906	2673
△	△	△	△	△	★	★	★	-7.897	2160
△	△	△	△	△	△	★	★	-7.768	1647
△	△	△	△	△	△	△	★	-6.285	1134
△	△	△	△	△	△	△	△	-0.011	450
★=LE-10Q9 model									
△= TE2 model									

Table 6: Displacement at point A for different structural models, Load case 1..

provide a reliable solution.

Figure 21 shows the evolution of the error related to u_z^B with respect to the number of DOFs. Figure 21a is related to the first load case. The diagram shows the slow convergence of the TE models with respect to LE models. The node-dependent kinematic models are able to speed-up the convergence and to ensure accurate result with only the 50% of the DOFs used by the uniform kinematic LE models .

Figure 21b shows the error in the case of the second load case. This figure shows that in the second case the use of a node dependent kinematic is no more convenient because the global deformation requires a refined model everywhere. In this case the homogeneous LE models are required in order to achieve an accurate solution.

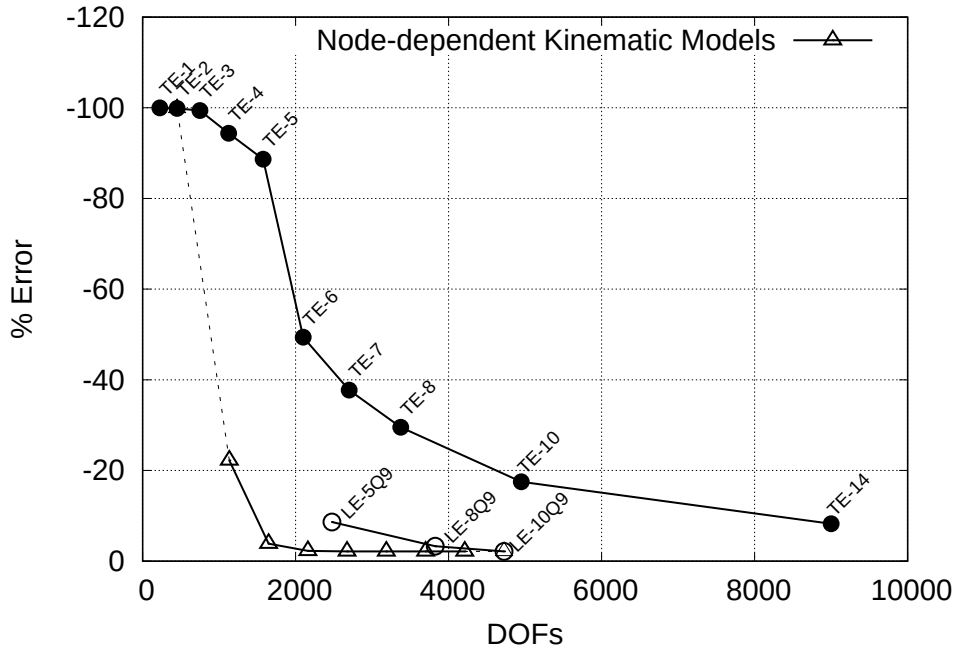

(a) Load case 1

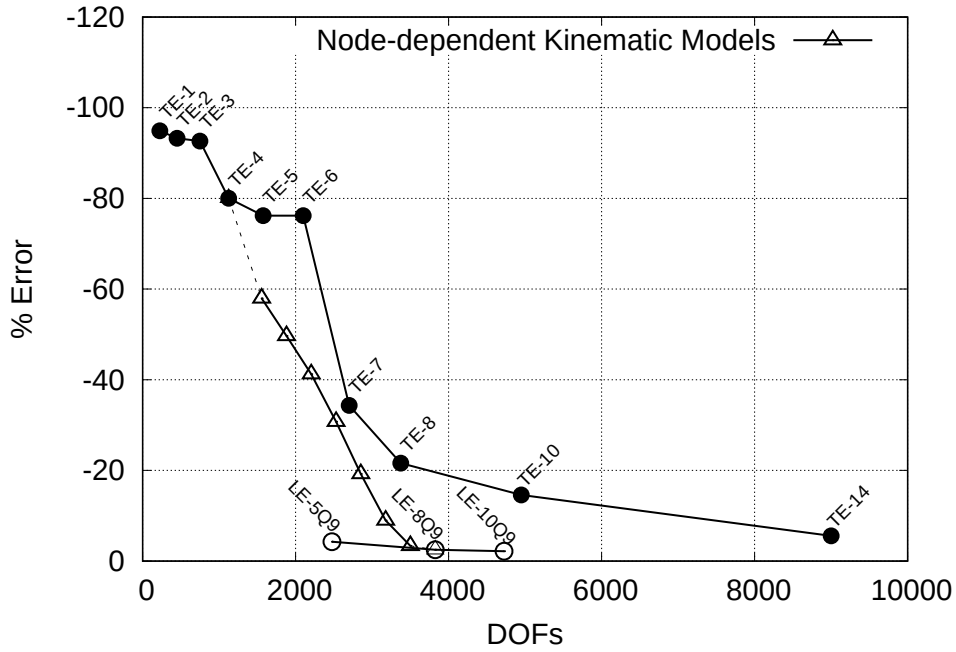

(b) Load case 1

Figure 21: u_z^A percentage error with respect the reference solution.

Structural model for each element										
El.1	El.2	El.3	El.4	El.5	El.6	El.7	El.8	$u_A \times 10^{-2}$[m]	$u_B \times 10^{-2}$[m]	NDOF
★	★	★	★	★	★	★	★	-1.931	-2.712	3825
△	★	★	★	★	★	★	★	-1.906	-2.688	3501
△	△	★	★	★	★	★	★	-1.751	-2.532	3177
△	△	△	★	★	★	★	★	-1.465	-2.247	2853
△	△	△	△	★	★	★	★	-1.145	-1.926	2529
△	△	△	△	△	★	★	★	-0.854	-1.634	2205
△	△	△	△	△	△	★	★	-0.628	-1.400	1881
△	△	△	△	△	△	△	★	-0.505	-1.169	1557
△	△	△	△	△	△	△	△	-0.510	-0.555	1125
★=LE-8Q9 model										
△= TE-4 model										

Table 7: Displacement at points A and B for different structural models, Load case 2.

5. Conclusions

The present paper presents a unified formulation for the development of a node-dependent kinematic beam element. The use of the Carrera Unified Formulation allows finite element matrices to be written in a compact and general form. The capabilities of this tool have been used to develop a node-dependent kinematic model that allows different kinematic models do be used at each node of the beam element. Unlike the traditional techniques used to couple different kinematic models, the present approach does not require any ad hoc formulation and just uses the FEM properties. The node-dependent kinematic model was first assessed in the analysis of a compact cross-section beam and then in the static analysis of a thin-walled structure. The results have been correlated with the computational costs in order to highlight the improvement in performances of constant kinematic models. The following considerations can be drawn from the obtained results:

- The node-dependent kinematic elements can be derived in the CUF framework, without the use of a specific approach, such as the Arlequin

Method or Lagrange Multipliers.

- Node-dependent kinematic elements allow a different kinematic model to be used at each node of the structure.
- The use of node-dependent kinematic elements allows refined models to be used only where they are required.
- The variation in the kinematics allows the number of unknowns to be reduced, because refined models are only used where they are really needed.

In short, the present node-dependent kinematic model can be considered a breakthrough with respect to uniform kinematic elements. The use of these elements could lead to benefits in several applications, such as in the analysis of local effects, global to local analyses, variable section beams and when beam should be connected to other structural models.

References

Ambrosini, R., 2000. A modified Vlasov theory for dynamic analysis of thin-walled and variable open section beams. Engineering Structures 22 (8), 890–900.

Babuska, I., Chandra, J., 1984. Adaptive Computational Methods for Partial Differential Equations. SIAM, Philadelphia.

Bar-Yoseph, P., Avrashi, J., 1988. On the nature of the free edge stress singularity in composite laminated plates. International Journal for Numerical Methods in Engineering 26 (7), 1507–1523.

Bar-Yoseph, P., Ben-David, D., 1995. Free-edge effects in unsymmetrically laminated composite plates. Composite Structures 30 (1), 13–23.

Ben Dhia, H., 1998. Multiscale mechanical problems: the arlequin method. Comptes Rendus de l'Academie des Sciences Series IIB Mechanics Physics Astronomy 326 (12), 899–904.

Ben Dhia, H., Rateau, H., 2005. The arlequin method as a flexible engineering tool. International journal for numerical methods in engineering 62 (11), 1442–1462.

Berdichevsky, V. L., 1976. Equations of the theory of anisotropic inhomogeneous rods. Dokl. Akad. Nauk 228, 558–561.

Biscani, F., Giunta, G., Belouettar, S., Carrera, E., Hu, H., 2011. Variable kinematic beam elements coupled via Arlequin method. Composite Structures 93, 697–708.

Blanco, P. J., Feijóo, R. A., Urquiza, S. A., 2008. A variational approach for coupling kinematically incompatible structural models. Computer Methods in Applied Mechanics and Engineering 197 (17-18), 1577–1602.

Carrera, E., 1995. A class of two dimensional theories for multilayered plates analysis. Atti Accademia delle Scienze di Torino, Memorie Scienze Fisiche 19-20, 49–87.

Carrera, E., 2002. Theories and finite elements for multilayered, anisotropic, composite plates and shells. Archives of Computational Methods in Engineering 9 (2), 87–140.

Carrera, E., Cinefra, M., Petrolo, M., Zappino, E., 2014a. Finite Element Analysis of Structures Through Unified Formulation. John Wiley & Sons.

Carrera, E., Filippi, M., Zappino, E., 2014b. Free vibration analysis of laminated beam by polynomial, trigonometric, exponential and zig-zag theories. Journal of Composite Materials 48 (19), 2299–2316.

Carrera, E., Giunta, G., Nali, P., Petrolo, M., 2010. Refined beam elements with arbitrary cross-section geometries. Computers & Structures (88), 283–293.

Carrera, E., Pagani, A., Petrolo, M., 2013. Use of Lagrange multipliers to combine 1D variable kinematic finite elements. Computers & Structures 129, 194–206.

Carrera, E., Petrolo, M., 2011. On the effectiveness of higher-order terms in refined beam theories. Journal of Applied Mechanics 78 (2).

Carrera, E., Petrolo, M., Zappino, E., 2012a. Performance of CUF Approach to Analyze the Structural Behavior of Slender Bodies. J. Struct. Eng. 138, 285–297.

Carrera, E., Petrolo, M., Zappino, E., 2012b. Performance of CUF approach to analyze the structural behaviour of slender bodies. Journal of Structural Engineering 138 (2), 285–297.

Carrera, E., Zappino, E., November 1420 2014. Analysis of Complex Structures Coupling Variable Kinematics One-Dimensional Models. In: Proceedings of ASME 2014 International Mechanical Engineering Congress & Exposition. Montreal, Quebec, Canada.

Carrera, E., Zappino, E., 2016. Carrera Unified Formulation for Free-Vibration Analysis of Aircraft Structures. AIAA Journal 45 (1), 280–292.

Carrera E., Petrolo, M., 2012. Refined Beam Elements With Only Displacement Variables and Plate/Shell Capabilities. Meccanica 47 (3), 537–556.

Cowper, G. R., 1966. The Shear Coefficient in Timoshenko's Beam Theory. Journal of Applied Mechanics 33 (2), 335–340.

Davies, J. M., Leach, P., 1994. First-order generalised beam theory. Journal of Constructional Steel Research 31 (2-3), 187–220.

Davies, J. M., Leach, P., Heinz, D., 1994. Second-order generalised beam theory. Journal of Constructional Steel Research 31 (2-3), 221–241.

de Saint-Venant, A., 1856. Memoire sur la flexion des prismes, sur les glissements transversaux et longitudinaux qui l' accompagnent lorsqu'elle ne

s'opre pas uniformement ou en arc de cercle, et sur la forme courbe affectee alors par leurs sections transversales primitivement plan. Journal de Mathématiques pures et appliquées 1, 89–189.

Dong, S., Alpdogan, C., Taciroglu, E., jun 2010. Much ado about shear correction factors in Timoshenko beam theory. International Journal of Solids and Structures 47 (13), 1651–1665.

Euler, L., 1744. De curvis elasticis. Methodus inveniendi lineas curvas maximi minimive proprietate gaudentes, sive solutio problematis iso-perimetrici lattissimo sensu accepti.

Fish, J., 1992. The s-version of the finite element method. Computers & Structures 43 (3), 539–547.

Friberg, P. O., 1985. Beam element matrices derived from Vlasov's theory of open thin-walled elastic beams. International Journal for Numerical Methods in Engineering 21, 1205–1228.

Giavotto, V., Borri, M., Mantegazza, P., Ghiringhelli, G., Carmaschi, V., Maffioli, G. C., Mussi, F., 1983. Anisotropic beam theory and applications. Computers & Structures 16 (1), 403–413.

Horgan, C., Simmonds, J., 1994. Saint-Venant end effects in composite structures. Composites Engineering 4 (3), 279–286.

Lin, H. C., Dong, S. B., Kosmatka, J. B., 2001. On Saint-Venant's Problem for an Inhomogeneous, Anisotropic CylinderPart III: End Effects. Journal of Applied Mechanics 68 (3), 392.

Park, J. W., Hwang, J. W., Kim, Y. H., 2003. Efficient finite element analysis using mesh superposition technique. Finite Elements in Analysis and Design 39 (7), 619–638.

Prager, W., 1967. Recent Progress in Applied Mechanics. Almquist and Wiksell, Stockholm, Ch. Variational principles for linear elastostatics for discontinous displacements, strains and stresses.

Rachowicz, W., Oden, J. T., Demkowicz, L., 1989. Toward a universal h-p adaptive finite element strategy part 3. design of h-p meshes. Computer Methods in Applied Mechanics and Engineering 77 (12), 181–212.

Ransom, J. B., 2001. On multifunctional collaborative methods in engineering science. Ph.D. thesis, Langley Research Center.

Reddy, J. N., Robbins, D. H., 1994. Theories and computational models for composite laminates. Appl. Mech. Rev. 47 (6), 147–165.

Schardt, R., 1966. Eine Erweiterung der Technischen Biegetheorie zur Berech- nung Prismatischer Faltwerke. Der Stahlbau 35, 161–171.

Schulz, M., Filippou, F., 1998. Generalized warping torsion formulation. Journal of Engineering Mechanics 124 (3), 339–347.

Silvestre, N., Camotim, D., sep 2002. First-order generalised beam theory for arbitrary orthotropic materials. Thin-Walled Structures 40 (9), 791–820.

Szabo, R. E., Babuska, I., 1991. Finite element analysis. John Wiley & Sons Ltd.

Timoshenko, S. P., 1921. On the corrections for shear of the differential equation for transverse vibrations of prismatic bars. Philosophical Magazine 41, 744–746.

Tullini, N., nov 1997. Decay rate of Saint-Venant end effects for multilayered orthotropic strips. International Journal of Solids and Structures 34 (33-34), 4263–4280.

Vlasov, V. Z., 1961. Thin walled elastic beams.

Volovoi, V., mar 1999. Asymptotic theory for static behavior of elastic anisotropic I-beams. International Journal of Solids and Structures 36 (7), 1017–1043.

Washizu, K., 1968. Variational methods in elasticity and plasticity. Oxford: Pergamon Press.

Wenzel, C., 2014. Local FEM Analysis of Composite Beams and Plates: Free-Edge effect and Incompatible Kinematics Coupling. Ph.D. thesis, Universite Paris Ouest Nanterre La Defense - Politecnico di Torino.

Yoon, K., Lee, P.-S., 2014. Modeling the warping displacements for discontinuously varying arbitrary cross-section beams. Computers & Structures 131, 56–69.

Yoon, K., Lee, Y., Lee, P.-S., 2012. A continuum mechanics based 3-D beam finite element with warping displacements and its modeling capabilities. Structural Engineering and Mechanics 43 (4), 411–437.

Yu, W., Hodges, D. H., 2004. Asymptotic Approach for Thermoelastic Analysis of Laminated Composite Plates. Journal of Engineering Mechanics 130 (5), 531.

Yu, W., Volovoi, V. V., Hodges, D. H., Hong, X., 2002. Validation of the variational asymptotic beam sectional analysis. AIAA Journal 40, 2105–2113.

Živković, M., Kojić, M., Slavković, R., Grujović, N., 2001. A general beam finite element with deformable cross-section. Computer Methods in Applied Mechanics and Engineering 190 (2021), 2651–2680.